Electric Propulsion Activities at the UCLA Plasma & Space Propulsion Laboratory

IEPC-2019-547

Presented at the 36th International Electric Propulsion Conference
University of Vienna • Vienna, Austria
September 15-20, 2019

Richard E. Wirz[1], Adam L. Collins[2], Zhitong Chen[3], Cesar E. Huerta[4], Gary Z. Li[5], Stephen A. Samples[6], Anirudh Thuppul[7], Peter L. Wright[8], Nolan M. Uchizono[9], Henry Huh[10], McKenna J. Davis[11], Angelica Ottaviano[12]
University of California, Los Angeles, Los Angeles, California, 90095, USA

The Plasma & Space Propulsion Laboratory (PSPL) is part of the Wirz Research Group at the University of California, Los Angeles (UCLA). This paper highlights recent and ongoing efforts by current members of the lab related to Electric Propulsion research topics such as miniature ion thrusters, plasma material interactions, and electrospray thrusters. All efforts use a combination of theory, experiments, and computational modeling. The Miniature Xenon Ion (MiXI) is one of the first technologies from the lab; recent efforts have focused on ion thruster discharge physics and advancement and integration of key technologies for TRL advancement. Plasma Material Interactions (PMI) can significantly affect the performance and life of many current and future electric propulsion (EP) devices; recent efforts in the lab have focused on PMI science to understand the promise and challenges of new material options that can improve plasma discharge performance and may even lead to improved device lifetimes. Electrospray thrusters can provide extremely high thrust precision and increased mission capabilities; recent efforts at PSPL have focused on electrospray emission behavior and implications of this behavior on thruster performance and life.

[1] Professor, Mechanical and Aerospace Engineering, wirz@ucla.edu.
[2] Research Scientist, Department of Mechanical & Aerospace Engineering, collinsalc55@ucla.edu .
[3] Postdoctoral Scholar, Mechanical and Aerospace Engineering, zchen@ucla.edu.
[4] Ph.D. Candidate, Mechanical and Aerospace Engineering, ceshuer@ucla.edu.
[5] Ph.D. Candidate, Mechanical and Aerospace Engineering, gli@ucla.edu.
[6] Ph.D. Candidate, Mechanical and Aerospace Engineering, stephen.samples@ucla.edu.
[7] Ph.D. Candidate, Mechanical and Aerospace Engineering Department, athuppul@ucla.edu.
[8] Ph.D. Candidate, Mechanical and Aerospace Engineering Department, plloydwright@ucla.edu.
[9] Ph.D. Candidate, Mechanical and Aerospace Engineering Department, nuchizono@ucla.edu.
[10] Ph.D. Candidate, Department of Mechanical & Aerospace Engineering, henryhuh89@ucla.edu.
[11] Ph.D. Student, Department of Mechanical & Aerospace Engineering, mjdavis325@ucla.edu.
[12] Ph.D. Student, Department of Mechanical & Aerospace Engineering, angelica.ottaviano@ucla.edu.

Nomenclature

DC-ION	=	Direct Current Ion (plasma model)
ELM	=	Electrospray Life Model
HOAGIE	=	Highly Optimizable Apparatus for Ground-Breaking Investigations of Electrosprays
IIEE	=	Ion-Induced Electron Emission
IonIEE	=	Ion-Induced Electron Emission (model)
LAS	=	Laser Absorption Spectroscopy
LDM	=	Long Distance Microscope
LIF	=	Laser Induced Fluorescence
LISA	=	Laser Interferometer Space Antenna
LOS_A , LOS_E	=	Line-of-sight to the accelerator and extractor grids
MiXI	=	Miniature Xenon Ion (thruster)
MiXI(3-Ring)	=	MiXI thruster with 3-ring discharge
MiXI(ARCH)	=	MiXI thruster with Axial Ring Cusp Hybrid discharge
OES	=	Optical Emission Spectroscopy
Pi	=	Facility for Plasma interactions research
PMI	=	Plasma Material Interactions
PSPL	=	Plasma & Space Propulsion Laboratory (Wirz Research Group, UCLA)
PSPL-EHD	=	PSPL ElectroHydroDynamics (model for electrospray extraction physics)
SEE	=	Secondary Electron Emission
SEEM	=	Secondary Electron Emission Model
SPaDE	=	Sputtering and Deposition (model)
UCLA	=	University of California, Los Angeles
WRG	=	Wirz Research Group

I. Introduction

THE Plasma & Space Propulsion Laboratory was started in 2008 as part of the Wirz Research Group at the University of California, Los Angeles (UCLA), http://www.wirz.seas.ucla.edu/plasma. The following sections highlight recent and ongoing efforts by current members of the lab related to miniature ion thrusters, plasma material interactions, and electrospray thrusters.

II. Miniature Xenon Ion (MiXI) Thruster

The first successful noble gas miniature ion thruster was reported by Wirz, *et al.* starting in 2001 using a permanent magnet DC discharge [1] [2] [3] [4]. This thruster, which came to be known as the Miniature Xenon Ion (MiXI) thruster, shown in Figure 1, uses a 3-ring cusp DC discharge and advanced ion optics to achieve desirable total efficiency, up to 56%, very high propellant efficiency, up to 82%, and thrust levels over 1.5 mN. More recent efforts using miniaturized hollow cathodes showed that a self-heated cathode discharge could be achieved with similar performance [5]. The MiXI thruster was run in pulsed width modulated (PWM) mode and was able to consistently achieve an impulse bit of only 1 μN•s. [6].

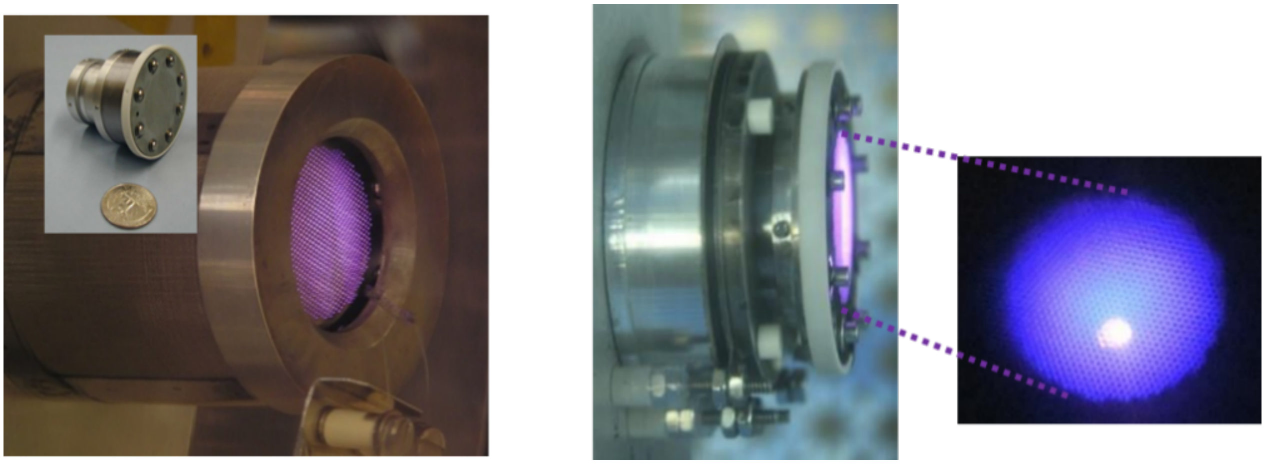

Figure 1. MiXI(3-Ring) provides desirable thrust performance and high-precision for lower-power (<50 W) space missions[left]. MiXI(ARCH) can provide higher discharge performance at higher power (50-100 W)[right].

A. **MiXI Thruster Development**

Recently, the MiXI thruster underwent an examination of discharge performance using experiments, computational models, and theory. This has led to two MiXI architectures shown in Figure 1: MiXI(3-Ring) is based off the original MiXI discharge and provides attractive performance for sub-50 W applications that desire high discharge stability, while MiXI(ARCH) provides higher performance in the 50-100 W range. The Axial Ring-Cusp Hybrid (ARCH) discharge was developed to examine methods to achieve higher discharge efficiency and exploits advantages from ring-cusp, Kaufman [7], and magneto-electrostatic thrusters [8] to effectively confine primary electrons, resulting in a highly efficient discharge with discharge utilization efficiencies as low as 226 W/A (Watts of discharge power / Beam current) [9] [10]. The ARCH discharge employs predominantly axial magnetic fields that effectively shield anode surfaces to prevent primary electron loss directly to the anode, while all cusp-terminating surfaces are biased to below cathode potential to electrostatically repel primary electrons. This results in a larger portion of primary electron energy being deposited into the plasma rather than lost to electrode surfaces [10].

MiXI is currently undergoing a Technology Readiness Level (TRL) increase effort to further develop the thruster with components and materials more appropriate for flight and to improve performance through discharge and cathode development. Thus far, this effort has included integration of hollow cathodes as discharge and neutralizer cathodes, development and integration of a novel discharge, and development of analytical tools. An analytical tool similar to [11] was developed to calculate internal plasma properties as a function of operating conditions and geometry. This tool has been compared with data and applied to identifying loss mechanisms and avenues for further discharge development [9]. Miniature hollow cathodes developed in [4] have been integrated into the thruster as discharge and neutralizer and are being characterized for total system performance. A low-flow BaO miniature hollow cathode has been characterized and installed in the MiXI(3-Ring) thruster for low power (25 - 45 W) operation. In parallel, a medium-flow BaO orificed hollow cathode has been installed in the MiXI(ARCH) thruster for operation in the 50-100 W power range. Characterization for both cathodes and discharges is ongoing.

B. MiXI Mission Analysis

Past mission studies have shown that MiXI fills a variety of mission-enabling roles such as primary propulsion for high-impulse microsatellite missions [12] [13] or as secondary propulsion for large spacecraft attitude control, station keeping, and formation flying [14]. As shown in Figure 2, recent mission studies for a 6U CubeSat with a 30 W MiXI reveal that the thruster provides up to 9 km/s mission ΔV for a 1U payload, and 4.3 km/s for a 3U payload. A notional 6 U mission with a 3U, 4 kg payload takes an estimated 50 weeks to generate 3 km/s mission ΔV. Neutralizer cathode performance was also shown to be an important consideration, with flowrate strongly affecting total system I_{sp} and power impacting total system power efficiency [15].

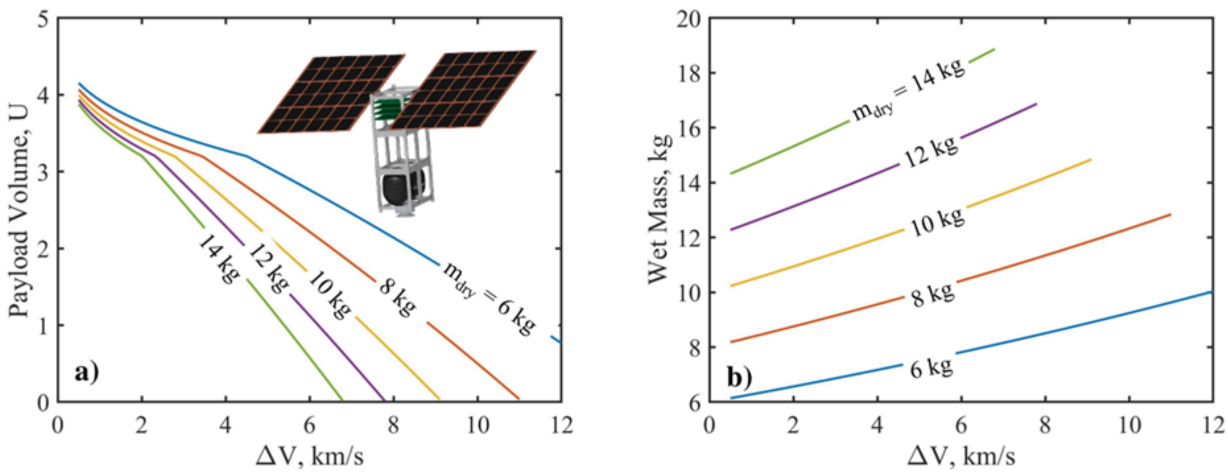

Figure 2. Payload volume (a) and wet mass (b) for a 6U CubeSat with a 30 W MiXI System as a function of mission ΔV and craft dry mass.

III. Plasma-Material Interactions for Electric Propulsion

Many EP devices require careful consideration of plasma interaction with thruster and spacecraft materials. These interactions are multi-faceted and often strongly coupled. As shown in Figure 3, the plasma interacts with the surface through the plasma sheath via photons, electrons, and ions. The bombardment of the surface can lead to material heating, erosion/damage, and property modification. The material interacts with the plasma via secondary electron emission (SEE), sputterants, and plasma ions that return to the plasma as neutrals. Overall, these species lead to plasma cooling, sheath modification, and contamination of the plasma, all of which can lead to reduced plasma performance.

These coupled interactions can be described in the following way. Ions, accelerated by the sheath, bombard plasma-facing surfaces and lead to sputtering of neutrals which can contaminate the plasma. These neutrals can also be ionized by electrons and redeposit onto surfaces, leading to increased downtime for fusion reactors. Sputtering of surfaces results in erosion, which for many devices, can limit the lifetime of certain components (tokamak divertors, ion thruster grids, etc.) and can also micro- or nano-roughen the surface. Secondary electron emission occurs when an energetic primary electron collides with a surface. The primary electron can then backscatter (either elastically or inelastically), or penetrate the surface and recoil wall electrons, which are emitted as true secondary electrons. SEE leads to a reduction in the sheath potential and plasma bulk electron temperature, as well as increased wall heat losses. In combination, these SEE effects could lead to a decrease in the rate of ionization in the plasma bulk.

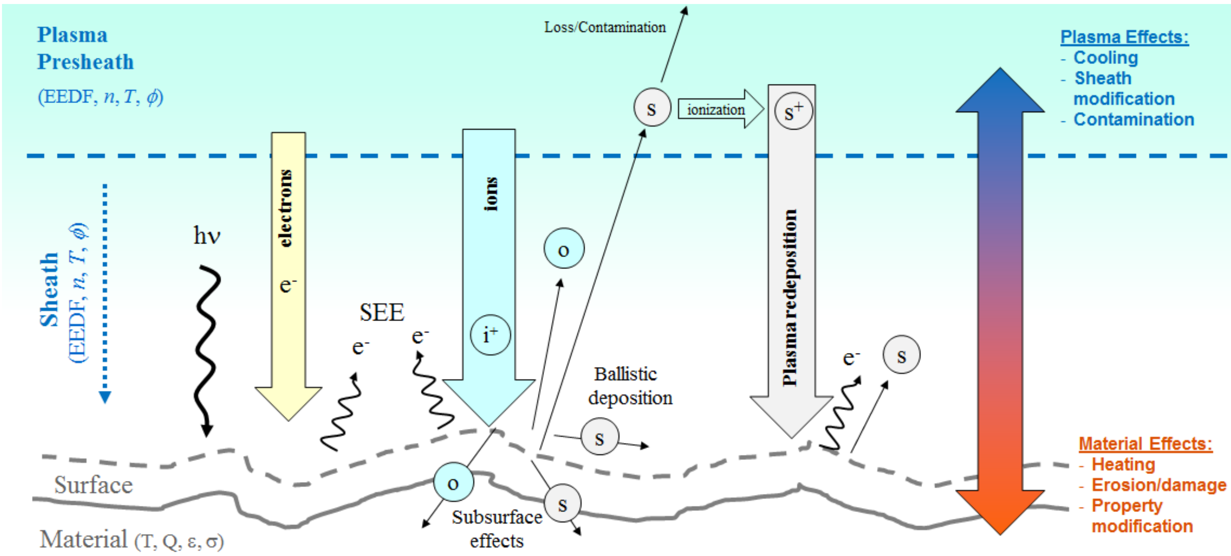

Figure 3: Interactions between plasma, surface, and sheath due to sputtering, deposition, redeposition, SEE, and IIEE. For the plasma, these interactions lead to plasma cooling, contamination, and modifications to the sheath potential. For the material, these interactions lead to heating of the surfaces, erosion, and physical damage.

A. PMI considerations for EP

Developing propulsion-grade and plasma-robust electrode materials is a crucial area of research for improving the performance and lifetime of electric propulsion (EP) devices [16]. Plasma-material interactions (PMI) occurring at the plasma-surface interface often cause unwanted effects in EP thrusters such as ion-induced sputtering, surface recession (erosion), core plasma contamination, and secondary electron emission (SEE) [17] [18]. Resolving PMI challenges can lead to prolonged thruster lifetimes, higher ΔVs for faster orbit transfers, and improved overall thruster efficiencies. In addition, designing materials with reduced erosion rates and reduced SEE yields can increase mission impulse by improving thruster performance and throttleability, leading to missions with higher agility. Plasma-robust electrodes can also enable high-power and high-thrust density propulsion systems such as magnetoplasmadynamic thrusters (MPDs) where high-density plasmas contact electrode surfaces, causing extreme erosion, vaporization, and material degradation. Leveraging PMI research from the magnetic confinement fusion community can provide insight for evaluating the complex PMI processes occurring in high-temperature and high-density plasma environments.

To this end, the Plasma & Space Propulsion Laboratory (PSPL) at the University of California, Los Angeles (UCLA) is investigating PMI processes and developing advanced electrode materials using state-of-the-art facilities and plasma and material diagnostics. Figure 4 shows how PMI processes impact different EP devices as well as facility effects. It is important to consider how a material affects the plasma parameters such as by plasma cooling and sheath modification, and how a plasma affects a material by electron, ion and photon bombardment, causing changes in the material properties. Investigating these coupled PMI processes is fundamental to improving thruster design and for enabling agile spacecraft.

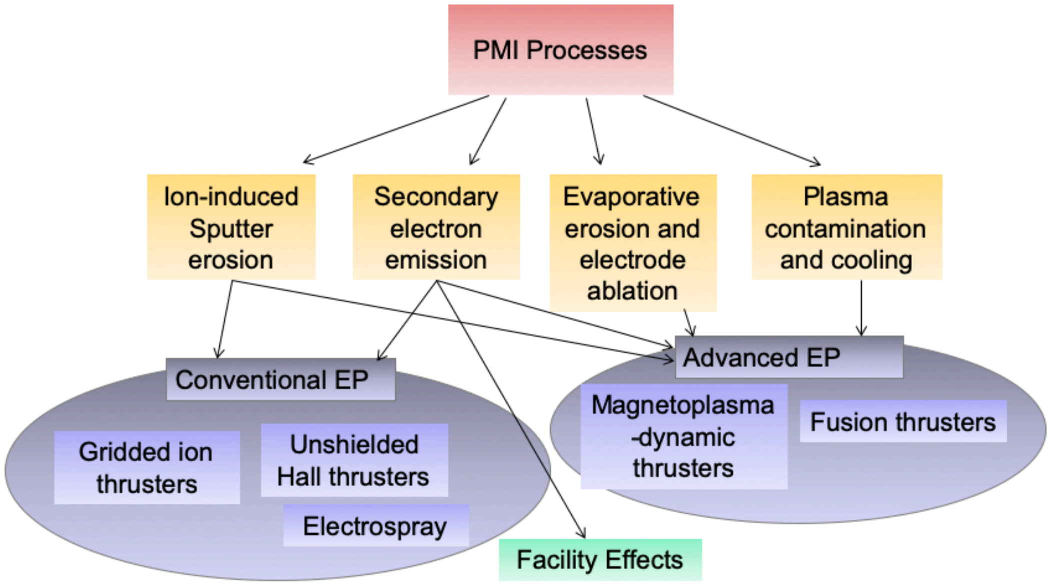

Figure 4. Summary diagram of PMI processes on different types of EP thrusters and testing. Note that "Secondary electron emission" includes the effects of electron-induced and ion-induced electron emission.

B. Experimental PMI Efforts

In-situ and *ex-situ* measurements are used to quantify plasma-material interactions (PMI) at the plasma-wall interface to assess the resilience of candidate materials and provide data for numerical simulations [19]. In addition to electrode erosion and deterioration, plasma interactions with materials can lead to impurity transport into the plasma core, which can cause ionization and excitation losses detrimental to overall thruster and system performance. To study these effects, plasma and material diagnostics will be fielded for *in-situ* and *ex-situ* analyses of the material response to the plasma in the UCLA Plasma Interactions (Pi) Facility as shown in Figure 5.

The Pi facility is a plasma column generated via a high current, 250 A max, LaB_6 hollow cathode and confined via solenoidal magnets. The downstream magnet shown in Figure 5 pinches down the magnetic field to provide focused plasma exposure to a material target. The target can be electrically biased relative to the local plasma potential, which is around ground potential, to provide energetic ion bombardment between 100 and 300 eV. Tested targets include commonly used EP materials (aluminum, carbon, etc.) and micro-engineered materials that may offer benefits for advanced EP concepts. In-situ diagnostics and representative results for the Pi Facility are shown in Figure 6, listed in Table 1.

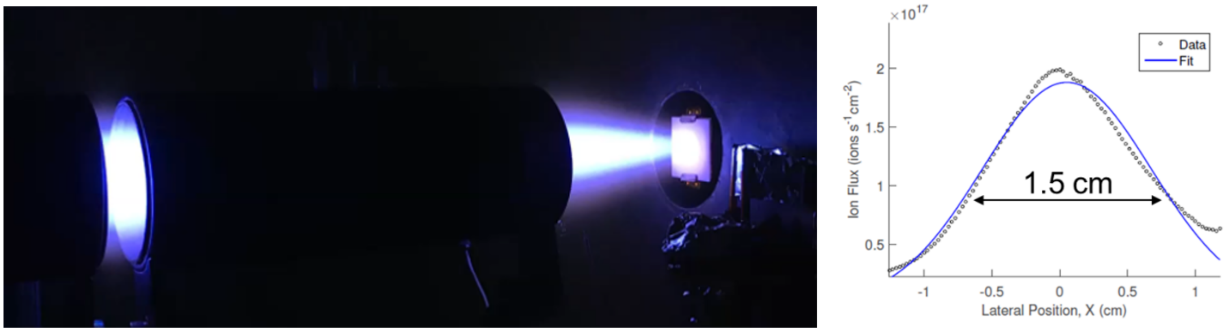

Figure 5. UCLA Plasma Interactions (Pi) Facility in operation [left]. The plasma is focused on the material target to concentrate exposure on the center of the specimen, however, a gradient of flux across the sample [right] allows each test to provide exposure for a wide range of plasma flux and fluence.

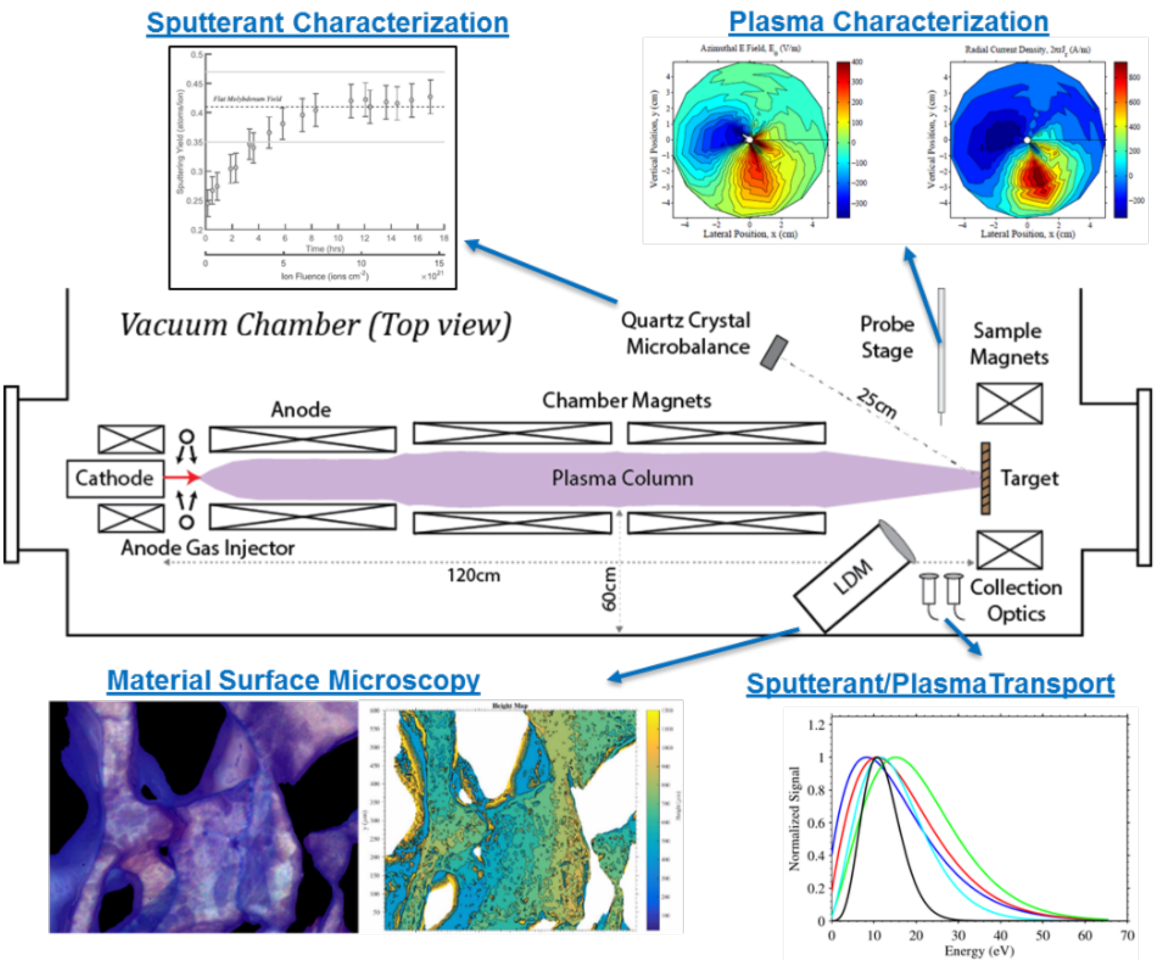

Figure 6. In-situ diagnostic setup for a biased material target in the PI facility at UCLA. The quartz crystal microbalance (QCM) provides sputtering rate characterization, the long-distance microscope (LDM) is used for real-time profilometry to assess material surface morphology, probes are used for plasma characterization, and collection optics are connected to optical emission spectroscopy (OES) and laser induced fluorescence (LIF) to capture plasma and sputterant transport.

Table 1. UCLA PMI diagnostics

Type	Diagnostic	Measured Parameters
Non-intrusive	Quartz Crystal Microbalance (QCM)	Differential sputtering rate, sputtering yield
	Long Distance Microscope (LDM)	Surface visualization, height map
	Optical Emission Spectroscopy (OES)	n_e, T_e and n_n of sputterant species
	Laser Induced Fluorescence (LIF)	Ion/neutral velocity distribution function
	Laser Absorption Spectroscopy (LAS)	n_n, T_n of sputterant species
Semi-intrusive	Langmuir Probe	n_e , T_e
	Faraday Probe	1-sided ion flux
	Emissive Probe	Plasma potential
	Retarding Potential Analyzer	Ion energy distribution
Ex-situ	SEM/EDS/TEM/XPS/Laser Profilometry	Comprehensive surface mapping

The quartz crystal microbalance (QCM) is a key diagnostic used to measure both the angular sputtering profile and total sputtering yield for a sputtered target in the Pi facility. If the scan duration is significantly less than the characteristic erosion time of a structured material, the time-resolved sputtering yield can be measured. Li, *et al*. [20] [21] measured the time-resolved sputtering yield of a structured molybdenum sample, showing that the sputtering yield was initially reduced but eventually approached the yield of a flat molybdenum surface.

Long distance microscopy (LDM) is used to acquire *in situ* visualization of the evolving surface morphology of a target material. Based on the LDM optics, surface features on the order of 100 um can be resolved and monitored over the course of a sputtering experiment. The image is captured via CCD and analyzed in Matlab to produce height maps of the structured surface. Efforts are underway to calibrate the height maps and obtain measurements of the surface recession speed during sputtering. In Figure 6, under the heading "Material Surface Microscopy", an in-situ microscopy image of eroding aluminum foam under argon plasma bombardment is shown. Next to this image is a height map of the features of the foam; the height map is obtained via in-situ focus variation profilometry from hundreds of images obtained by the LDM during in vacuo plasma exposure testing.

Plasma characterization in the Pi facility is done via a series of plasma diagnostics including Langmuir probes, Faraday probes, emissive probes, and RPAs. The density and temperature of the near-target plasma help to inform how the target material interacts with the plasma in terms of incident ion flux, plasma redeposition, and surface heating, among other phenomena. Matlock, *et al.* [22] measured rotating ion density regions in the near-target plasma as shown in the "Plasma Characterization" portion of Figure 6. These rotating structures may impact erosion measurements and also provide a canonical construct for the evaluation of plasma stability and transport investigations.

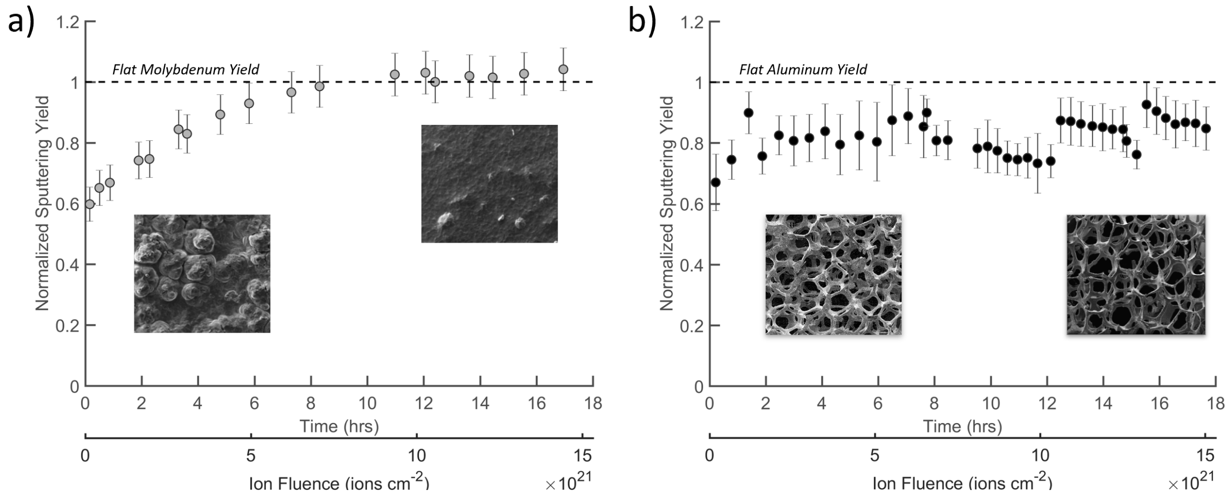

Figure 7. The left plot shows a) the sputtering yield of a structured molybdenum sample as a function of time and ion fluence over an 18 hr. exposure while the right plot shows b) the sputtering yield of a sample with an aluminum foam surface over the same time period.

Recent studies have shown that materials with featured surfaces such as velvets, grooved surfaces, foams and fuzzes are capable of trapping sputterants and secondary electrons in their inter-cavities [23]. One of the key results from Li, *et al.* [21] is that the sputtering yield of a structured molybdenum sample eventually approaches that of a flat molybdenum surface as shown in Figure 7a. Scanning Electron Microscopy (SEM) images confirm the evolution of the surface features towards a flat surface. The authors have discovered that the solution to the issue of temporary sputtering yield reduction is the use of a volumetrically structured material such as a foam. Figure 7b shows the total sputtering yield of a dual Al-Cu foam sample with the aluminum side facing the plasma. The sputtering yields for both plots are normalized to the flat sputtering yield at argon ion energies of 300 eV. The SEM images for the foam sample show that the entire field-of-view is composed of the foam pore structure, which eventually evolves into larger pores as the ligaments are gradually eroded away. However, since the overall structure of the foam is maintained throughout the sputtering process, the sputtering yield is reduced at a relatively steady value compared to that of the structured molybdenum sample.

The surface erosion of an aluminum foam has been investigated using a novel in-situ long distance microscopy (LDM) technique which uses focus-variation to reconstruct real-time composite images of a surface during argon 300 eV ion-bombardment. Figure 8 shows the material surface evolution during ion exposure for increasing ion fluence. The LDM diagnostic enables the visualization of surface changes such as foam ligament diameter reduction and flaking, which can cause plasma contamination in an EP device. Height maps can be generated to evaluate the erosion rate of the foam in conjunction with diagnostics for measuring the sputtering yield of the material. In the case of a foam surface, the erosion is comparable to that of a planar surface while the sputtering yield is reduced.

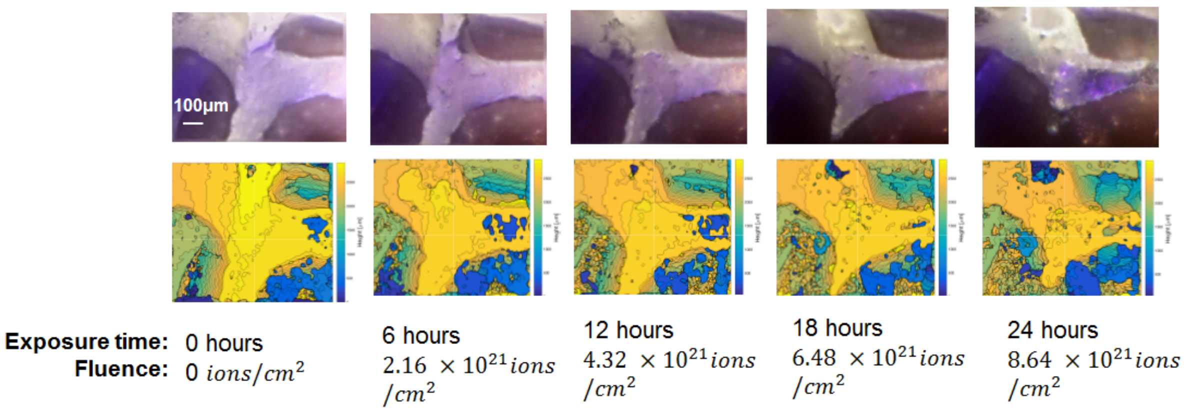

Figure 8. Composite images of an aluminum foam generated using in-situ LDM data and related height maps are shown for varying ion fluence during energetic argon ion bombardment.

While reduced sputtering is beneficial to reducing plasma contamination, further development is required to design materials with reduced erosion rates for prolonged electrode and thruster lifetimes. Approaches used in the magnetic confinement fusion community such as flowing liquid metals through foam surfaces for renewable plasma-facing components can be applied for EP-related PMI research. High current-density and temperature plasma environments are required for investigating fundamental PMI processes for the future development of advanced propulsion-grade electrodes.

C. Computational PMI Efforts

Along with diagnostic capabilities, UCLA has developed computational models to aid in understanding and simulating the interactions between plasma particles and surfaces. These models have separately focused on sputtering and erosion, secondary electron emission (SEE), and ion-induced electron emission (IIEE). Each model has been validated with data from both the literature, our own experiments, and collaborations. They are utilized to predict the effects of micro- and nano-scale surface texturing on these interactions.

The Sputtering and Deposition (SPaDE) model employs a view factor approach for computational efficiency to track the ballistic trajectory of incident ions and emitted sputterants [24] [25]. Simulations were carried out to assess the effects of surface texturing on the sputter yield as the emitted neutrals deposited onto neighboring surfaces. Modeling results were used to explain the hysteresis in previous sputtering observations and the growth of pillar-like deformations in fabricated nano-scale surfaces. As shown on Figure 9, protuberant pillars were shown computationally to play a significant role in suppressing the sputter yield above what was expected analytically due to their radial growth via deposition from sputtering of nearby nano rods.

The Secondary Electron Emission Model (SEEM) and the Ion Induced Electron Emission (IonIEE) model use Monte Carlo particle tracking and simplifications of complex, chaotic surface architectures to investigate the geometric effects these surfaces have on electron emission yield [26] [27]. These models have been validated with data from the literature, as well as our own, and aided in understanding the electron emission yield characteristics from tungsten fuzz and carbon velvet. As shown on Figure 10, the yield from tungsten fuzz does not depend on the incidence angle due to increased trapping of emitted secondary electrons by the horizontal fibers. This effect compensates the increase in the SEE yield by a surface due to the incidence angle and was confirmed computationally.

These models are currently being integrated with our plasma model, DC-ION, to more closely investigate the effects of plasma-material interactions (PMI) on a well-characterized plasma column interacting with an anode surface. DC-ION is a flexible hybrid plasma model which has been previously used to successfully simulate and design conventional and miniature ion thrusters. By using a combination of physics-based treatments, the model will reveal the effects that foam surfaces have on plasma properties, and in turn, how these effects on the plasma influence PMI physics. The advantageous properties of plasma-robust surfaces studied at UCLA can be applied to high power density fusion applications to reduce heat losses to the walls, decrease plasma contamination, and maintain high plasma densities (see Figure 3).

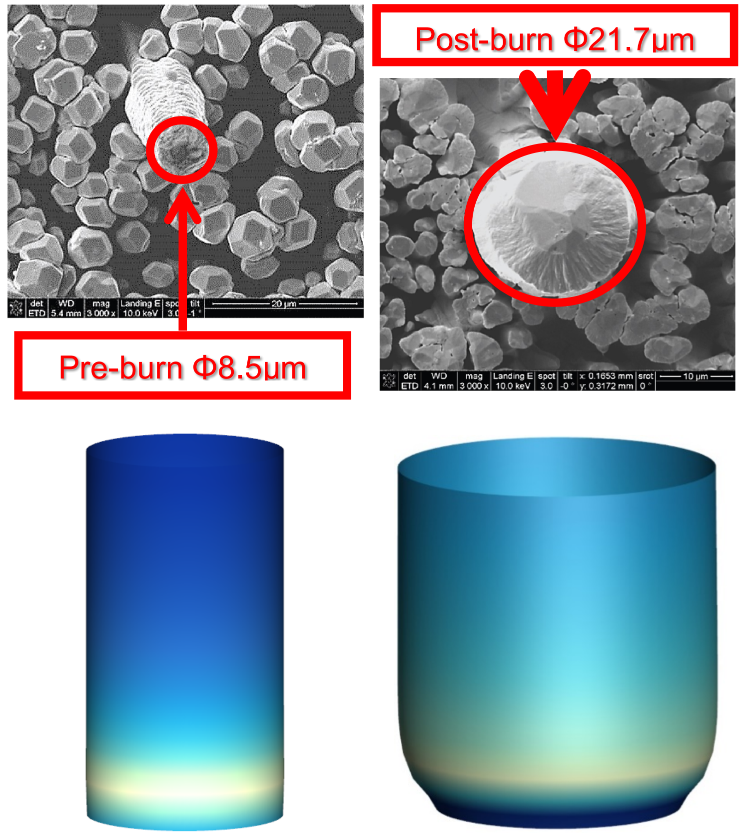

Figure 9: Simulation results for sputtering. The sputtering model simulated the radial growth of a protuberant pillar on a surface of nano rods after 2 hours of ion bombardment and confirmed its role in the increased suppression of sputtering.

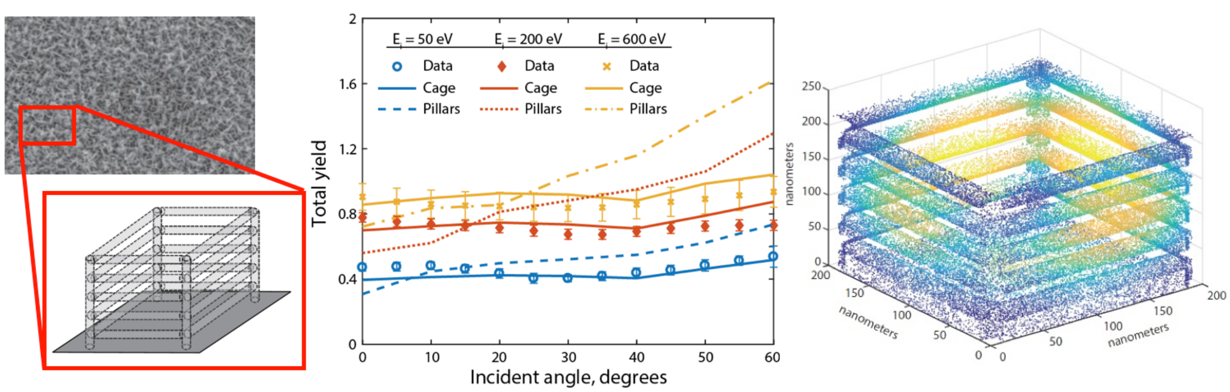

Figure 10: The SEE model shows that the lack of dependence of the SEE yield on incidence angle is due to the horizontal fibers observed in tungsten fuzz and represented by a cage-like geometry.

IV. Electrospray Thruster Research Activities

The Laser Interferometer Space Antenna (LISA) plans to use electrospray thrusters for precision position control for several tens of thousands of hours. To validate such long lifetime operation, the University of California, Los Angeles (UCLA) Plasma & Space Propulsion Laboratory (PSPL) is using a combination of analytical life modeling, computational modeling, and single emitter testing to analyze the implications of both steady and unsteady electrospray behavior on lifetime [28]. The present effort is part of the LISA Colloid Microthruster (CMT) development led by NASA JPL and in collaboration with Busek. The Electrospray Life Model (ELM) is used as a framework to estimate lifetime based on information from existing data/results and to inform ongoing experiments and modeling. The Highly Optimizable Apparatus for Groundbreaking Investigations of Electrosprays (HOAGIE) facility is used to investigate various aspects of capillary electrospray operation. Experimental results obtained from HOAGIE use a combination of current and mass flux monitoring with high-speed microscopy to understand the behavior of steady and unsteady modes and to estimate mass flux to the grids. Computational models are being used to examine electrospray behavior in four overlapping regions: The Extraction Region (cone-jet), the Transition Region (jet-to-droplet/ion), the Interaction Region (where interspecies Coulombic forces dominate), and the Plume Region. The complementary modeling and experimental efforts have revealed several important features of thruster operation, their implications on thruster lifetime, and necessary pathways for future investigations towards ensuring electrospray life and performance. In addition to supporting the LISA CMT effort, UCLA is developing advanced electrospray thruster concepts. A hybrid-emitter design has demonstrated the ability to achieve either ion-mode or droplet-mode emission. The following sections describe the electrospray propulsion research efforts at UCLA.

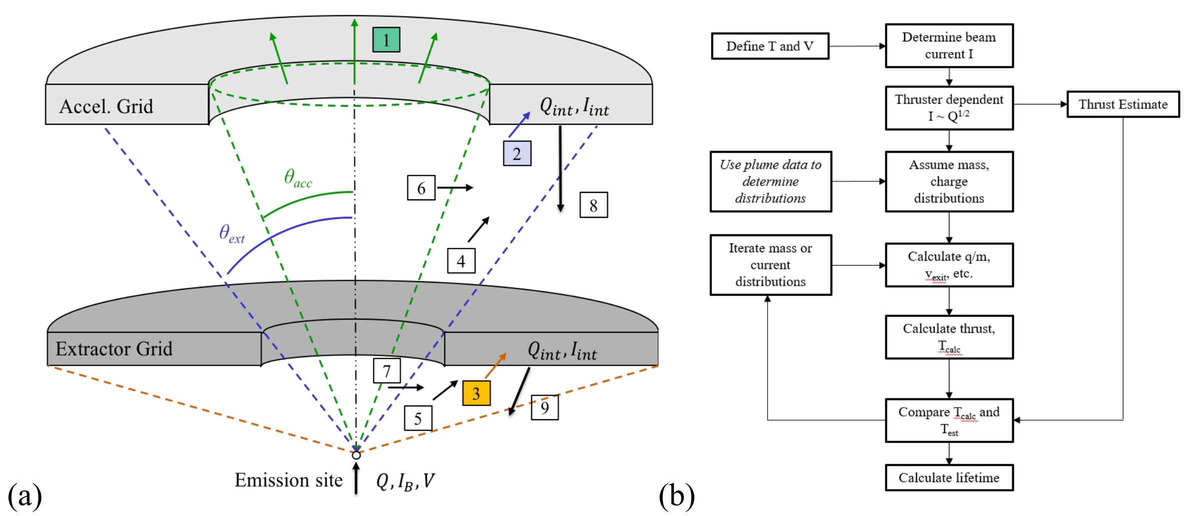

Figure. 11: (a) Emission from an electrospray that passes through the accelerator grid produces thrust (1). However, emission far off-axis ($\theta > \theta_{acc}$) results in grid impingement on the accelerator (2) and extractor grids (3). The off-axis emission can be categorized as a combination of direct overspray (4, 5) from the emission site and expansion of the beam (6, 7). As ionic liquid collects on or in the grid, the strong electric fields can cause backspray emission of propellant (8, 9) upstream towards the emitter in the region between the grids. (b) Description of grid impingement life model [28].

A. Electrospray Life Model

The Electrospray Life Model (ELM) is a continually-progressing analytical model used to make first order estimates of thruster life and performance using literature, experiments, and computational models. Resulting estimates and uncertainty inform ongoing experimental efforts and computational models to find pathways for reducing uncertainty in the life/performance estimations and reveal design and operational pathways for improving lifetime.

ELM uses information from in-house and outside sources to provide up-to-date estimates of failure probability. Failure mechanisms are added as they are identified, and their calculated probability of occurrence combined into the total lifetime calculation. Figure. 11 shows the process for grid saturation as described in Thuppul, *et al.* [29], whereby integration of an assumed Gaussian distribution of mass for a steady electrospray plume is shown to lead to propellant-saturation of the accelerator grid (the identified primary failure mechanism) in 17,000 - 38,000 hours, accounting for component tolerances. Additional failure mechanisms, such as transient spray modes leading to stochastic grid impingement, are treated with a similar analysis, with their individual failure probability distributions added together to provide a total lifetime estimate.

A key result from experimental testing and analyses is that the mass flux and current density of the plume do not share the same distribution [30], which has implications for how the plume would be accelerated as the charge-to-mass ratio is what matters. Furthermore, while the current density is almost Gaussian in nature, the mass flux profiles exhibit a flat-top distribution and a much sharper drop-off with half-angle (θ) than that of a Gaussian over many thrust and voltage setpoints. These mass flux data can be well fit with a Super-Gaussian profile. Figure 12 shows a Gaussian mass flux ($n = 1$), and Super-Gaussian mass flux ($n = 3.82$), each having the same width ($b = 27.3°$) and total flux. The sharply decaying mass-flux with half-angle is beneficial for lifetime, because the tails of the distribution contain much less mass than would be expected for a Gaussian plume of similar width, and hence the accelerator and extractor grid impingement rates would be expected to be much lower for steady operating conditions.

The thrust from the accelerated plume in both cases was calculated to be 2.9 μN, but the larger tail of the Gaussian plume beyond the accelerator aperture (highlighted in purple) and extractor aperture (highlighted in yellow) results in a much larger grid-impingement than for the Super-Gaussian-fit plume and hence substantially reduced lifetime. The accelerator is successful in reducing the amount of propellant impinging on the grids, but the Gaussian plume still shows substantially more flux beyond the accelerator line-of-sight (LOS_A). Indeed, when the mass flux is integrated beyond LOS_A to calculate the propellant accumulation rate and estimated lifetime (as in Thuppul, *et al.* [28]), the Gaussian plume case is estimated to reach grid saturation failure after ~15,000 hours with the Super-Gaussian plume reporting $\sim10^{189}$ hours of life (or more realistically, well beyond the required lifetime of the thruster).

Even at higher flow rates where plumes expand to larger half-angles [30], the probability of grid-impingement is very small over a large range of operating conditions, due to the rapid decay of mass flux with polar angle (as measured at UCLA PSPL) and tightening of the plume with acceleration. Therefore, life estimates using these mass-flux profiles show that steady-state on-axis emission does not provide enough propellant to saturate the grids through overspray to limit lifetime [32].

Phenomenology from the experimental results and analysis of Wright, Thuppul, and Wirz [33] with further modeling-based analysis from Davis, Collins, and Wirz [32] suggests that overspray conditions (i.e. wide particle trajectories) will occur when negative velocity gradients are produced at emission. The stability of EMI-Im emission shown by Uchizono, *et al.* indicates that during steady emission such velocity disparities, arising from break-up instabilities, [33] are suppressed, and as such steady emission is not expected to produce excessive overspray.

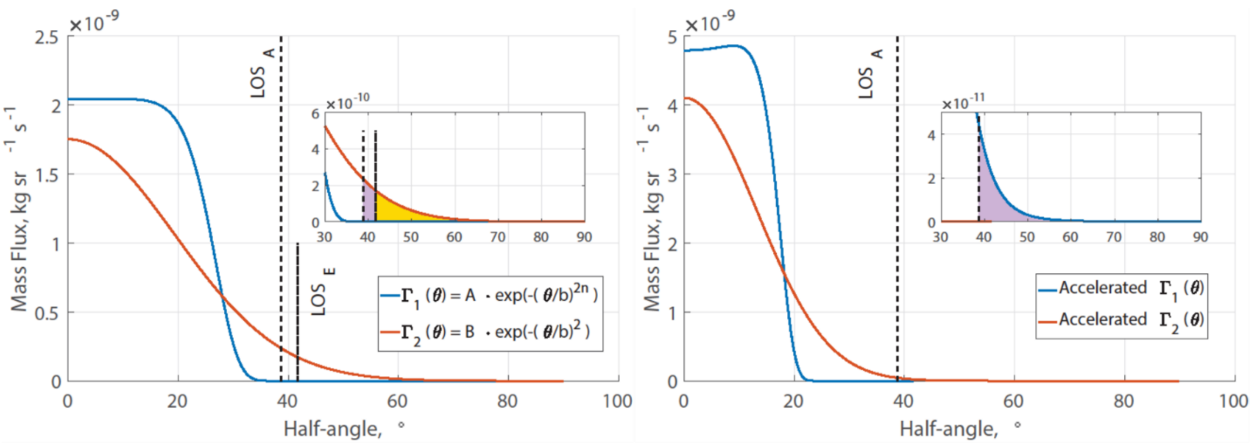

Figure 12: Super-Gaussian (blue, n = 3.82) and Gaussian (red, n = 1) mass flux profiles. Left: input mass flux profiles. Right: accelerated mass flux profiles. Plumes have the same width (b = 27.3 º) and total mass flux. The insets show the much larger propagation of the Gaussian profile beyond the extractor and accelerator aperture line of sight angles (LOS_E and LOS_A).

B. Electrospray Experimental Efforts

UCLA PSPL uses a single emitter as a conical construct for evaluating electrospray emission behavior and investigating extraction and plume evolution physics. Plume characterization of a single emitter is performed via high spatial resolution current and mass flux measurements across a wide range of angles [30]. During operation, a probe armature was swept through the electrospray plume to obtain current and mass profiles via a spherical electrostatic probe and a Quartz Crystal Microbalance (QCM), respectively. A long-distance microscope (LDM), with additional optics, observed the electrospray during operation.

Figure 13 shows that the mass flux and current exhibit non-Gaussian behavior. The mass flux profiles have a flatter top, and their width increases with flow rate. These trends are easily observed in the polar plots in Figure 14, where the peak mass flux shifts to higher half-angles with increasing flow rate, indicating a broadening plume width. The mass flux profile is slightly sensitive to emitter voltage with off-axis emission apparent at high emitter voltages. The resulting charge-to-mass ratio profiles indicate that heavier droplets are primarily located in the central region of the plume, whereas the wide regions are primarily composed of ions and smaller droplets. The mass and current plume measurements are designed to explain observed electrospray phenomena across a wide range of electrospray systems. Plume data is used in conjunction with theory and computational modeling to inform life and performance estimations for electrospray systems.

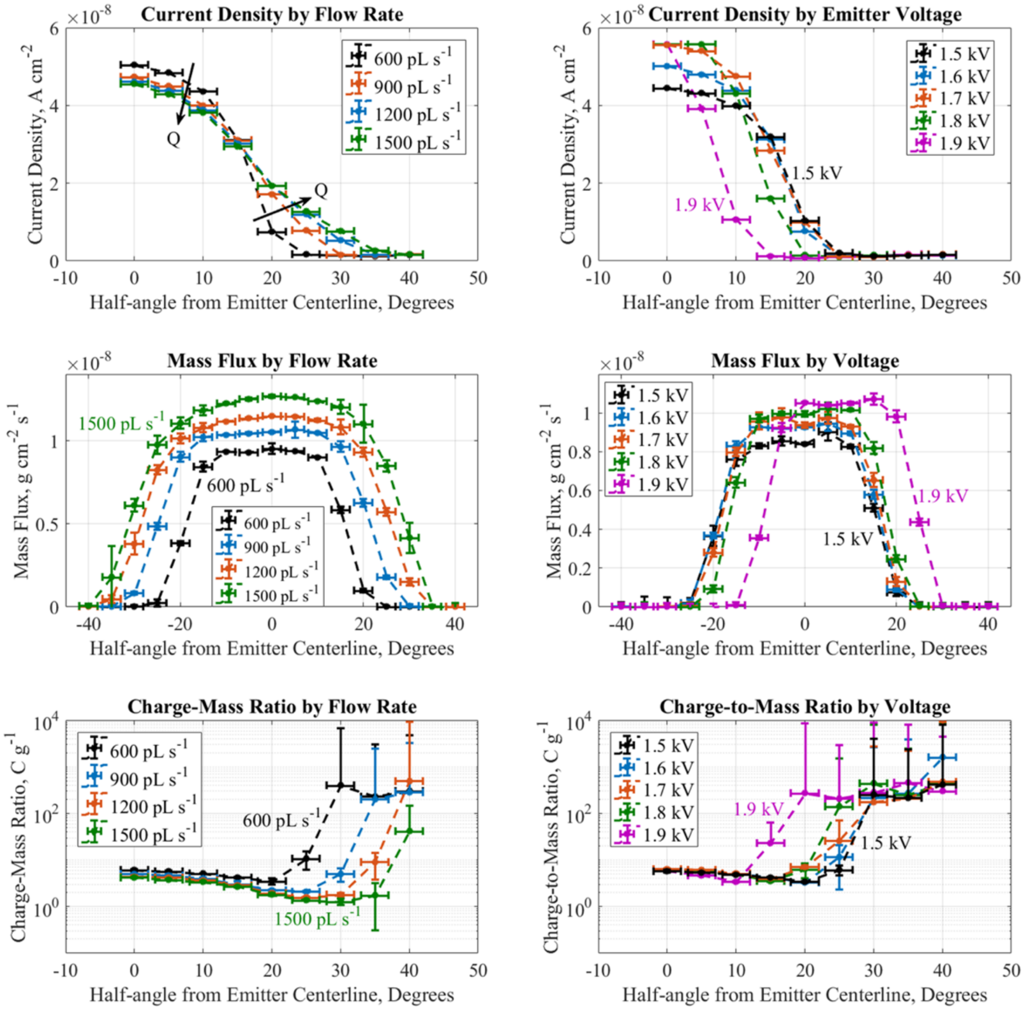

Figure 13: Measurements of mass flux, current, and charge-mass ratio profiles at varying flow rate and emitter voltage setpoints taken as the probe mount is angularly swept across the center of the plume.

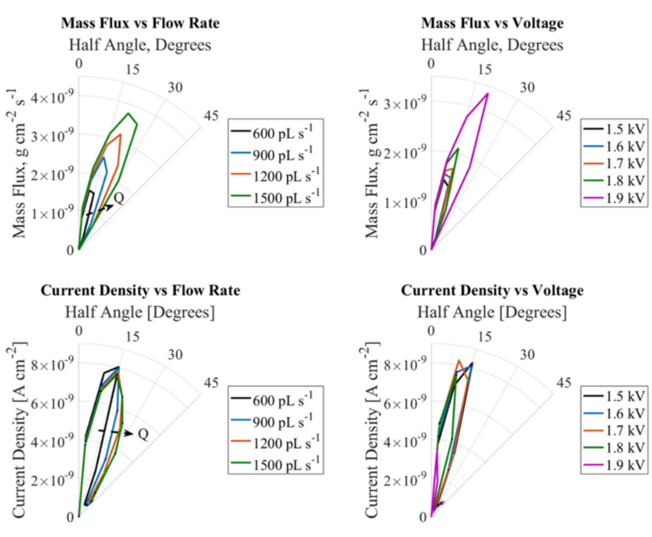

Figure 14: Polar plots of mass flux and current density for varying flow rates and emitter voltages.

As discussed in the ELM overview, the presented plume data indicates that steady-state on-axis emission does not appreciably contribute to electrospray thruster lifetime. However, unstable emission modes may result in significant grid impingement [31], so characterizing electrospray emission stability is critical to estimating and improving the lifetime of electrospray propulsion devices. Steady-state stability experiments have been performed on an EMI-Im electrospray over flow rates from 400 pL/s to 1300 pL/s, and extraction voltages from 1.3 kV to 2.0 kV [33]. Images of the emission site are shown in Figure 15.

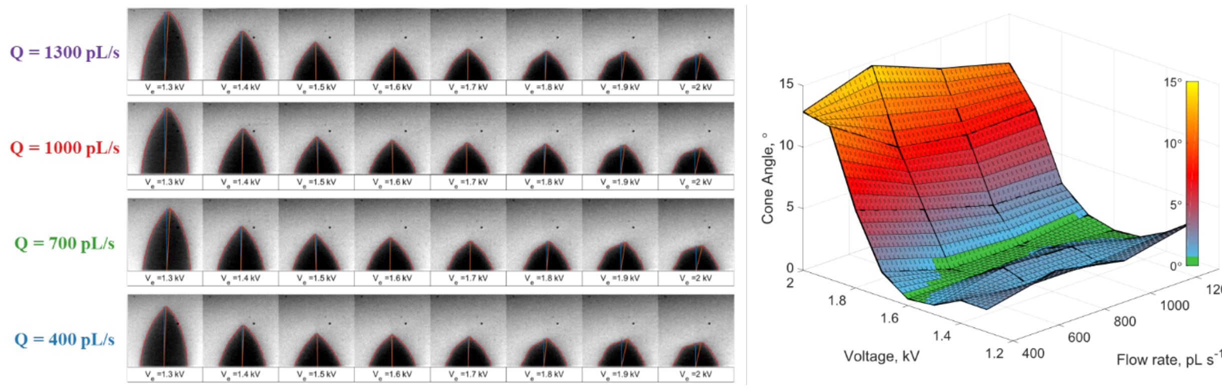

Figure 15: Spatial Instabilities of Steady-State Electrospray Emission. Left: Images of the electrified meniscus over the emission map. Flow rates range from 400 - 1300 pL/s and voltages range from 1.3 - 2.0 kV. No unsteady modes are observed, but off-axis emission angle appears to vary with emission parameters. Right: A 3D mapping of off-axis emission angle. A clear trough, suggesting high spatial stability for emission, is observed at 1.6 kV across all flow rates.

No temporal emission instabilities were observed in the steady-state emission stability test. Instead, stable off-axis emission was observed at the upper and lower bounds of the voltage setpoints. The off-axis emission behavior observed at the emission site follow the trends seen in the plume's mass profiles downstream. When compared to ethanol electrospray stability [31], EMI-Im emission is apparently much more stable, which may be attributed to the substantially higher viscosity and conductivity of EMI-Im. Barrerro, *et al.* [34] reported that azimuthal instabilities in the cone's internal flow are suppressed at Reynolds numbers less than unity, defined by:

$$Re = \frac{\rho U d_n}{\mu} = \left[\frac{\gamma \varepsilon_0 \rho^2 I^2}{d_n K^2 \mu^4}\right]^{\frac{1}{2}} \tag{4}$$

Where γ is surface tension, ε_0 is the permittivity of free space, ρ is density of the fluid, I is the emitter current, d_n is the inner diameter of the capillary, K is the conductivity of the fluid, and μ is the viscosity of the fluid. For the given geometry in the presented stability experiments, Re was calculated to be ~ 10^{-5}, which indicates that helical motion in the cone is suppressed. Additionally, increased stability of the electrified jet was analytically demonstrated by Hohman, *et al.* [35], and experimentally observed by Nayak, *et al.* [36].

Transient stability tests were also performed using EMI-Im, where startup and shutdown of emission were tested in nominal and off-nominal conditions. Nominal startup conditions involve applying a constant extraction voltage, while ramping the flow up and down. Off-nominal startup conditions involve applying constant flow rate, and rapidly applying or removing an extraction voltage. The nominal startup, nominal shutdown, and off-nominal shutdown all occurred with no observed unstable transients. However, during off-nominal startup, extremely unstable pulsating behavior was observed. A sequence of stills from the off-nominal startup emission are shown in Figure 16.

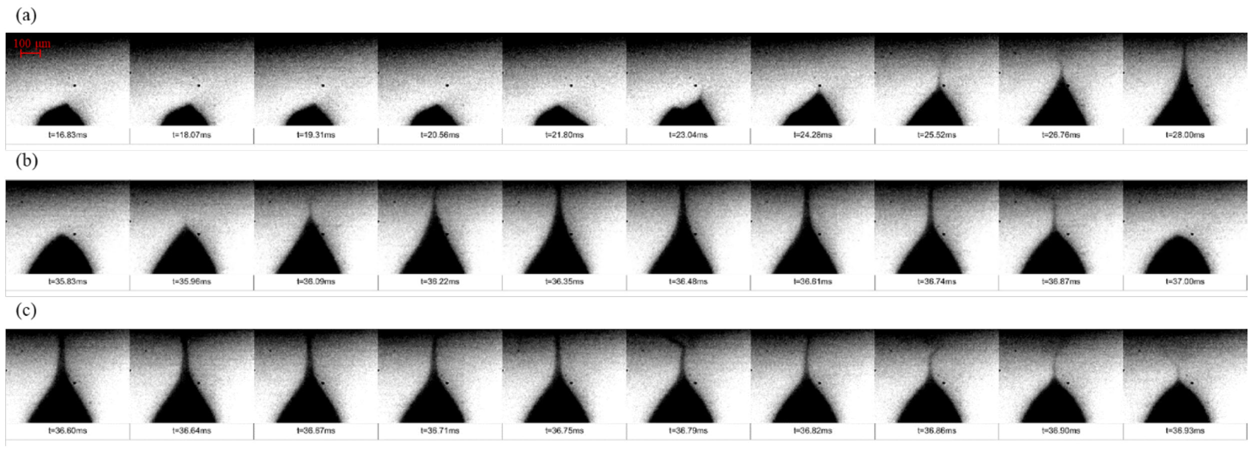

Figure 16: Off-nominal startup image sequences, 1300 pL/s flow rate, 0 kV to 1.6 kV emitter bias. (a) Onset of emission transient. Two cones merge into a single emission site that immediately begins pulsating. (b) Single cycle of pulsation after onset of emission. (c) Whipping jet instability that occurs during relaxation period of the pulsation cycle.

During the off-nominal startup test, flow was held at a constant 1300 pL/s prior to applying the 1.6 kV extraction bias. A pulsation of approximately 1 kHz was observed for several hundred milliseconds. Eventually, the electrospray reached a steady cone-jet emission mode. We hypothesize that a large amount of propellant had accumulated on the emitter prior to application of the extraction voltage. Therefore, once voltage was applied, an artificially elevated propellant flow rate was delivered to the emission site. The pulsation instability eventually settles to a steady cone-jet mode once the excess propellant is cleared from the emission site. While EMI-Im exhibits greater stability than other less viscous and less conductive fluids, certain operating modes may still enable unstable operation, resulting in reduced lifetime.

C. Electrospray Computational Efforts

Computational modeling is critical to understand electrospray emission and plume evolution for steady and transient operating conditions. To capture life limiting effects such as grid impingement, it is important to develop modeling capabilities that resolve unsteady and time-dependent effects. To capture the wide range of physical mechanisms that participate in the development of an electrospray plume, we discretize the computational domain into distinct regions, as shown in Figure 17. The computational regions are distinguished as follows:

1. Extraction Region: The electrostatic force overcomes the fluid surface tension to form a cone-jet and generate droplets. The simulation for the region utilizes computational fluid dynamics (CFD) analysis under incompressible and axisymmetric assumptions.
2. Transition Region: Coulombic fission and ion evaporation cause off-axis behavior of droplets.
3. Interaction Region: Droplet breakup and inter-particle Coulombic interactions cause the plume to expand.
4. Plume Region: Coulombic interactions no longer dominate the particle dynamics.

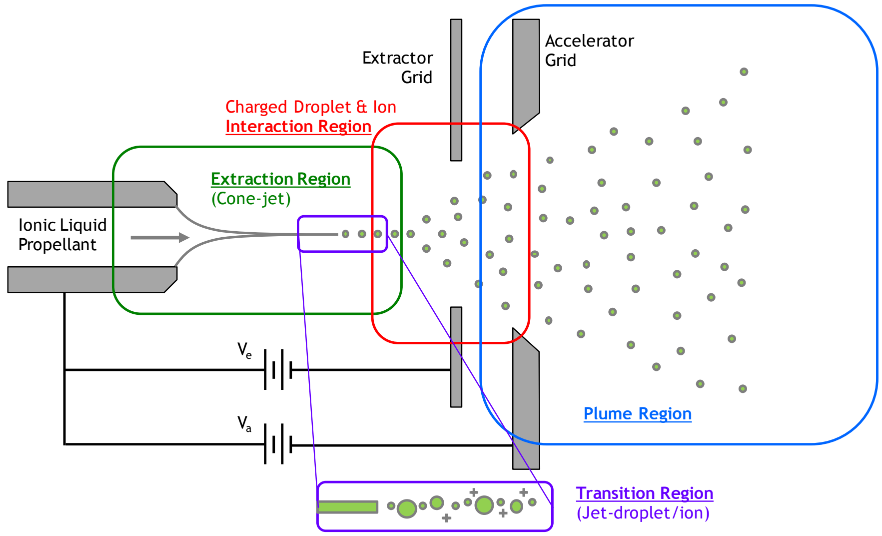

Figure 17: Electrospray computational domains.

The Extraction Region of the electrospray computational domain is modelled using the Plasma & Space Propulsion Laboratory's Electro-Hydro-Dynamic (PSPL-EHD) model based on the electrowetting model to understand the physics of a cone-jet and droplet formation of an electrospray thruster [37] [38]. By applying the governing equations without major simplifying assumptions to the model, PSPL-EHD was able to capture unsteady behaviors and instabilities of the liquids during extraction in electrospray modeling [38].

In Figure 18, the electric field magnitude distribution is depicted in time. This figure shows that the electrostatic force induced from electric field is a main contributing factor along with charge density according to Eq. 1:

$$\vec{F_e} = \rho_e \vec{E} - \tfrac{1}{2}\vec{E}^2 \nabla \varepsilon \qquad (1)$$

where $\vec{F_e}$ is electrostatic force, $\vec{E}$ is electric field, ρ_e is charge density, and ε is electrical permittivity. As can also be seen in Fig. 3, electric field is the highest at time $t_d = 0.4$ ms where charge conduction is transitioning to charge convection. UCLA-PSPL is currently investigating this transition region to understand the physics and to develop the model for observing unsteady behaviors and

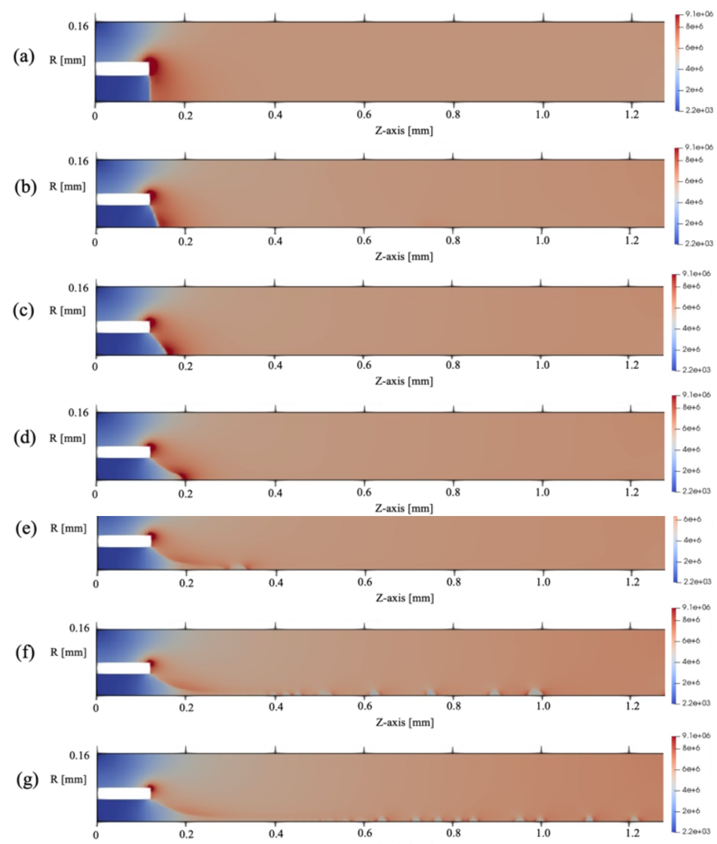

Figure 18: Electric field magnitude distribution in extraction region at start up condition. (a) $t_a = 0.1\ ms$, (b) $t_b = 0.2\ ms$, (c) $t_c = 0.3\ ms$, (d) $t_d = 0.4\ ms$, (e) $t_e = 0.5\ ms$, (f) $t_f = 0.6\ ms$, (g) $t_g = 3.7\ ms$ (steady).

instabilities. These behaviors are critical for high conductivity extractions using EMI-Im as a propellant for the electrospray thruster.

The Interaction Region of the electrospray computational domain is simulated using the Interaction Model – a discrete element, particle-pushing model that was developed in-house [32]. The Interaction Model simulates electrospray droplet dynamics immediately downstream of the Transition Region, through expansion into the Plume Region. Each electrospray droplet is treated as a rigid point charge subjected to Coulombic interactions with neighboring droplets, an applied electric field, drag, and gravity (Eq. 2). These forces are visually depicted in

Figure 19.

$$F_d = \sum_{i=0}^{N-1} k\frac{q_d q_i}{r_{d,i}^2} + q_d E + \frac{\pi r_d^2 \rho C_D (U - v_d)^2}{2} + g m_d, \quad (2)$$

Simulation results corroborate experimental discoveries and accompanying theory that showed negative velocity gradients for emitted droplet species provoke "traffic jams" with resulting large-magnitude Coulombic interactions that facilitate plume expansion [31] [32]. These "traffic jams" can occur in inhomogeneous electrospray plumes because droplets are electrostatically accelerated according to their specific charge. Therefore, smaller, high specific charge droplets are accelerated into larger, lower specific charge droplets and undergo Coulombic interactions which repel the small droplets to wide plume angles. Plumes simulated in the Interaction Model show the propensity of electrosprays to angularly segregate themselves according to droplet specific charge. Such a plume shape is demonstrated visually and via cumulative mass, charge, and modal plume profiles (Figure 20) for a plume composed of 3 discrete droplet species from the literature [39].

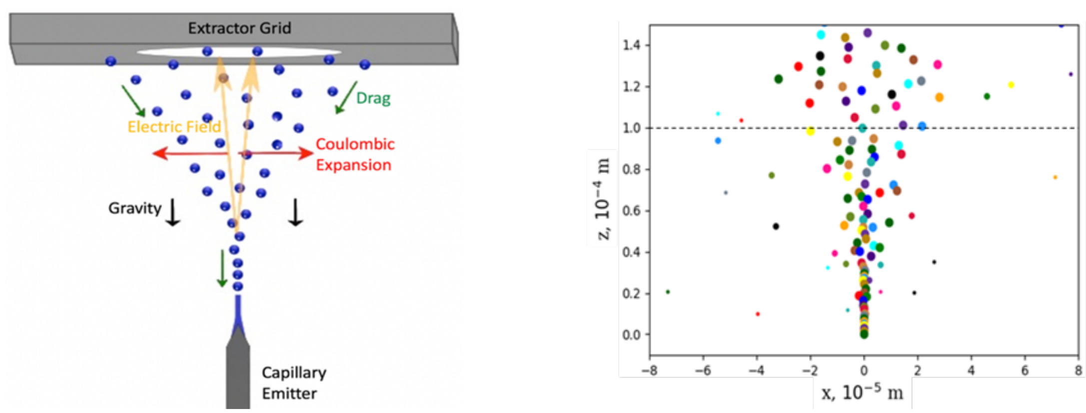

Figure 19: (Left) Coulombic, electric field, gravitational, and drag forces act on droplets in the plume. (Right) A plume simulated in the Interaction Model comprised of 3 droplet species (Small, Medium, and Large) from the literature [39]. A dashed line signifies the height at which profiles displayed in Figure 20 were measured.

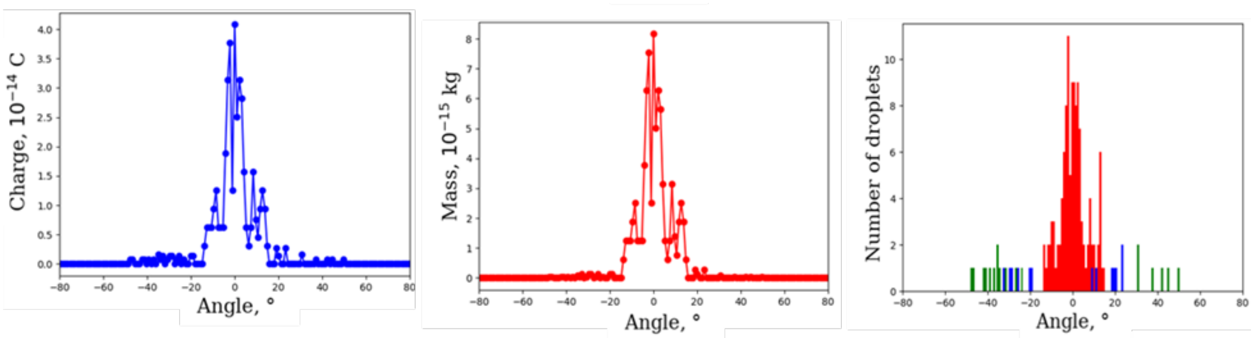

Figure 20: Evolution of a plume comprised of 3 droplet species (Small, Medium, and Large). For the complete plume displayed in Figure 19, (left) cumulative charge, (middle) cumulative mass, and (right) cumulative frequency profiles are shown for the distance from emission marked in Figure 19 by a dashed line. In the right-side plot, droplets are divided into three species, with red representing the Large droplets, blue for Medium droplets, and green for the Small droplets. Figures are adapted from Davis, et al. [32]

D. Advanced Electrospray Concepts

A novel geometry of electrospray emitter has been developed for achieving dual-mode propulsion. The design takes advantage of the natural increase in specific charge of emission as current decreases to produce high specific impulse operation at low flow rates and high thrust-to-power operation at high flow rates. A needle in the center of a capillary emitter promotes stable emission at low flow rate in an externally wetted emission mode. When flow rate is increased, the meniscus extends past the needle to emit in a capillary or cone-jet mode.

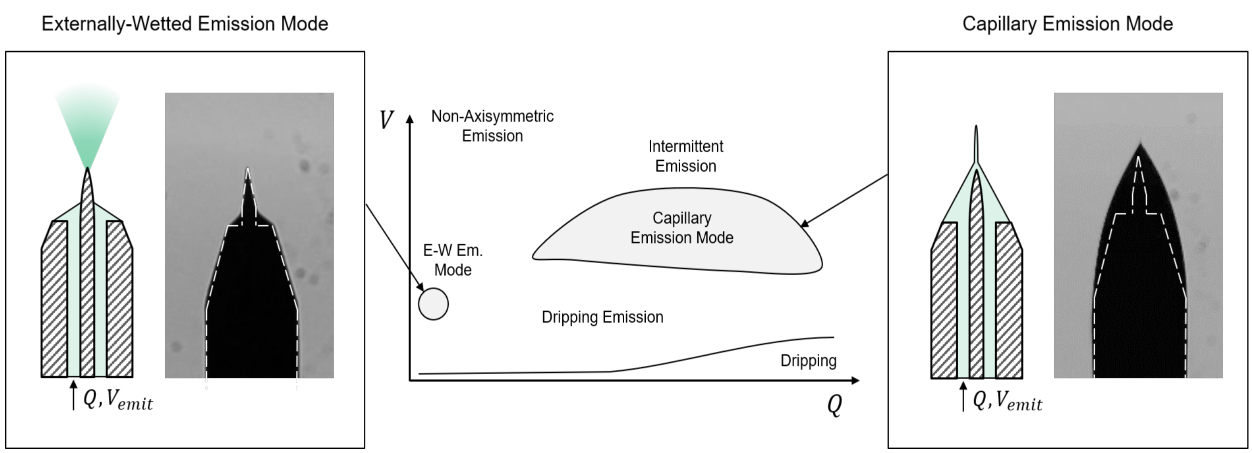

Figure 21: The operating regimes for the hybrid emitter, adapted from Chen [41]. Characteristic still images and diagrams of each emission mode are shown.

Emission from a meniscus staked to the capillary was achieved by commanding high flow rates of 2.4 to 2.8 nL/s while operating at an emitter voltage of 1.5 kV. High flow rates were required to extend the meniscus past the needle such that the two did not intersect. To emit at low flow rates, the emitter was operated in an externally-wetted emission mode. Driving flow rate is reduced to a negligible level and propellant flows to the tip of the needle due to a combination of surface wettability, capillary forces and Maxwell pressure effects. Recorded emission current for this operating mode was 2 nA. Based on the operating conditions leading to capillary emission and externally-wetted emission modes, we propose a stability plot as shown in Figure 21. The externally-wetted and capillary emission modes are distinct and separated by unstable operating modes. The concept of a variable emission mode electrospray device has been validated experimentally. A more detailed explanation of the design, as well as experimental and computational results can be seen in Wright, *et al.* [42].

V. Conclusion

The Plasma & Space Propulsion Laboratory (PSPL) conducts research on several electric propulsion (EP) topics including miniature ion thrusters, plasma material interactions, and electrospray thrusters. All efforts use a combination of theory, experiments, and computational modeling. The Miniature Xenon Ion (MiXI) is one of the first technologies from the lab; recent efforts have focused on ion thruster discharge physics and advancement and integration of key technologies for TRL advancement. Plasma Material Interactions (PMI) can significantly affect the performance and life of many current and future electric propulsion (EP) devices; recent efforts in the lab have focused on PMI science to understand the promise and challenges of new material options that can improve plasma discharge performance and may even lead to improved device lifetimes. Electrospray thrusters can provide extremely high thrust precision and increased mission capabilities; recent efforts at PSPL have focused on electrospray emission behavior and implications of this behavior on thruster performance and life.

Acknowledgments

The authors would like to thank the efforts of the alumni of the Wirz Research Group and their support of past and current efforts in the Plasma & Space Propulsion Lab at UCLA. We would also like to thank our funding sources, including AFOSR, NASA, AFRL, JPL, NSF, and DoD. Current MiXI work is being funded by NASA Space Technology Research Fellowship NSTRF Grant #80NSSC17K0076. Recent PMI efforts have been supported by AFOSR Award Nos. FA9550-14-10317 (UCLA Subaward No. 60796566-114411) and FA9550-16-1-0444. Recent electrospray efforts have been supported by NASA/JPL Award No. 1580267 and AFRL 16-EPA-RQ-09.

VI. References

[1] R. E. Wirz, J. Polk, C. Marrese, J. Mueller, J. Escobendo and P. Sheehan, "Development and Testing of a 3 cm Electron Bombardment Micro-Ion Thruster," in *International Electric Propulsion Conference, IEPC-01-343*, Pasadena, 2001.

[2] R. E. Wirz, J. Polk, C. Marrese and J. Mueller, "Experimental and Conputational Investigation of the Performance of Micro-Ion Thruster," in *38th Joint Propulsion Conference, AIAA-2002-3835*, Indianapolis, 2002.

[3] R. E. Wirz, D. Goebel, C. Marrese and J. Mueller, "Development of Cathode Technologies for a Miniature Ion Thruster," in *39th AIAA Joint Propulsion Conference, AIAA-2003-4722*, Huntsville, 2003.

[4] R. E. Wirz, Discharge plasma processes in ring-cusp ion thrusters, Pasadena: California Insittute of Technology, 2005.

[5] R. E. Wirz, "Low Contamination, High-Precision Thruster for Precision Formation Flying Missions," JPL Report #R.06.023.065, 2006.

[6] R. E. Wirz, M. Gamero and D. Goebel, "Pulsed Operation of an Ion Accelerator," NASA Tech Brief 33(2), NPO-44961, pp. 24 , Pasadena, Feb 2009.

[7] H. R. Kaufman, Technology of Electron-Bombardment Ion Thrusters, Fort Collins: Academic Press, 1975.

[8] R. Moore, "Magneto-electrostatically contained plasma ion thruster," in *7th Electric Propulsion Conference, 1969-260*, 1969.

[9] S. A. Samples and R. E. Wirz, "Beam Extraction Performance Characterization of the MiXI Thruster with an ARCH Discharge," *Journal of Physics D,* Submitted 2019.

[10] B. Dankongkakul and R. E. Wirz, "Axial Ring-Cusp Hybrid (ARCH) plasma discharge: an approach to highly efficient miniature-scale ion sources," *Plasma Sources Science and Technology,* vol. 27, no. 12, 2018.

[11] D. M. Goebel, R. E. Wirz and I. Katz, "Analytical Ion Thruster Discharge Model," *Journal of Propulsion and Power,* pp. 1055-1067, 2007.

[12] R. W. Conversano and R. E. Wirz, "Mission Capability Assessment of CubeSats Using an Miniature Ion Thruster," *Journal of Spacecraft and Rockets,* pp. 1035-1046, 2013.

[13] R. E. Wirz, "Miniature Ion Thrusters: A Review of Modern Technologies and Mission Capabilities," in *34th International Electric Propulsion Conference, IEPC-2015-275*, Kobe, Japan, 2015.

[14] S. Martin, D. P. Scharf, W. R. E., O. Lay, D. McKinstry, B. Mennesson, G. Purcell, J. Rodrugiez, L. Scherr, J. R. Smith and L. Wayne, "Design Study for a Planet-Finding Space Interferometer," in *IEEE Aerospace Conference, AERO.2008.4526410*, 2008.

[15] S. A. Samples and R. E. Wirz, "Parametric Study of High Impulse CubeSat Mission Capabilities," *Spacecraft and Rockets,* Submitted 2019.

[16] R. E. Wirz, J. R. Anderson, D. M. Goebel and I. Katz, "Decel Grid Effects on Ion Thruster Grid Erosion," *IEEE Transactions on Plasma Science,* vol. 36, no. 0093-3813, 2008.

[17] R. E. Wirz, "Coupled Analysis of Ion Thruster Grid Erosion and Electron Backstreaming," *Space Propulsion 2010, San Sebastian.*

[18] Y. Raitses, A. Smirnov, D. Staack and N. J. Fisch, "Measurements of secondary electron emission effects in the Hall thruster discharge," *Physics of Plasmas,* vol. 13, no. 014502, 2006.

[19] T. S. Matlock, D. M. Goebel, R. Conversano and R. E. Wirz, "A dc plasma source for plasma-material interactions experiments," *Plasma Sources Science and Technology,* vol. 23, no. 025014, p. 11pp, 2014.

[20] G. Z. Li, C. A. Dodson, R. E. Wirz, T. S. Matlock and D. M. Goebel, "Implementation of in situ diagnostics for sputter yield measurements in a focused plasma," in *52nd Joint Propulsion Conference*, Salt Lake City, UT, 2016-4841.

[21] G. Z. Li, T. S. Matlock, D. M. Goebel, C. A. Dodson, C. S. R. Matthes, N. M. Ghoniem and R. E. Wirz, "In situ plasma sputtering and angular distribution measurements for structured molybdenum surfaces," *Plasma Sources Science and Technology,* vol. 26, no. 065002, p. 11pp, 2017.

[22] T. S. Matlock, C. A. Dodson, D. M. Goebel and R. E. Wirz, "Measurements of Transport due to Low Frequency Oscillations in a Rotating Hollow Cathode Plasma," in *34th International Electric Propulsion Conference*, Kobe, Japan, 2015-137.

[23] G. Z. Li, T. S. Matlock, D. M. Goebel, C. A. Dodson, C. S. R. Matthes, N. M. Ghoniem and R. E. Wirz, "In situ plasma sputtering and angular distribution measurements for structured molybdenum surfaces," *Plasma Sources Sci. Technol ,* vol. 26, no. 065002, 2017.

[24] C. E. Huerta, T. S. Matlock and R. E. Wirz, "Validation of a Plasma-Facing Surface Sputtering and," in *AIAA SPACE 2015 Conference and Exposition*, 2015.

[25] C. E. Huerta, T. S. Matlock and R. E. Wirz, "View factor modeling of sputter-deposition on micron-scale-architectured surfaces exposed to plasma," *Journal of Applied Physics,* vol. 119, no. 11, p. 113303, 2016.

[26] C. E. Huerta and R. E. Wirz, "Surface geometry effects on secondary electron emission via Monte Carlo modeling," in *52nd AIAA/SAE/ASEE Joint Propulsion Conference*, 2016.

[27] C. E. Huerta and R. E. Wirz, "Secondary electron emission from textured surfaces," *Journal of Physics D: Applied Physics,* vol. 51, no. 14, p. 145202, 2018.

[28] R. E. Wirz, A. L. Collins, A. Thuppul, P. L. Wright, N. M. Uchizono, H. Huh, M. J. Davis, J. K. Ziemer and N. R. Demmons, "Electrospray Thruster Performance and Lifetime Investigation for the LISA Mission," in *AIAA 2019-3816, 2019 Propulsion and Energy Forum*, Indianapolis, IN, 2019.

[29] A. Thuppul, P. Wright, J. Ziemer and R. E. Wirz, "Lifetime Considerations for Electrospray Thrusters.," *Journal of Propulsion and Power,* 2019.

[30] K. Gillen-Christandl, G. D. Gillen, M. J. Piotrowicz and M. Saffman, "Comparison of Gaussian and super Gaussian laser beams for addressing atomic qubits.," *Applied Physics B 122.5,* p. 131, 2016.

[31] A. Thuppul, A. L. Collins, P. L. Wright, N. M. Uchizono and R. E. Wirz, "Spatially-Resolved Mass Flux and Current Measurements for Electrospray Plumes," in *IEPC-2019-571, 36th International Electric Propulsion Conference*, Vienna, Austria, 2019.

[32] A. L. Collins, A. Thuppul, P. L. Wright, N. M. Uchizono, H. Huh, M. Davis and R. E. Wirz, "Assessment of Grid Impingement for Electrospray Thruster Lifetime," in *IEPC-2019-213, 36th International Electric Propulsion Conference*, Vienna, Austria, 2019.

[33] P. L. Wright, A. Thuppul and R. E. Wirz, "Life-Limiting Emission Modes for Electrospray Thrusters," in *AIAA 2018-4726.c1, 54th AIAA/ASME/SAE/ASEE Joint Propulsion Conference & Exhibit*, Cincinnati, OH, 2018.

[34] M. J. Davis, A. L. Collins and R. E. Wirz, "Electrospray Plume Evolution via Discrete Simulations," in *IEPC-2019-590, 36th International Electric Propulsion Conference*, Vienna, Austria, 2019.

[35] N. M. Uchizono, A. L. Collins, D. Q. Eckhardt, A. Thuppul, P. L. Wright, R. E. Wirz and J. K. Ziemer, "High-Speed Electrospray Emission Behavior," in *36th International Electric Propulsion Conference*, Vienna, Austria, 2019.

[36] P. L. Wright, A. Thuppul and R. E. Wirz, "Life-Limiting Emission Modes for Electrospray Thrusters," in *54th AIAA/ASME/SAE/ASEE Joint Propulsion Conference & Exhibit, AIAA 2018-4726*, Cincinnati, OH, 2018.

[37] A. Barrero, A. M. Gañán-Calvo, J. Davila, A. Palacios and E. Gomez-Gonzales, "The Role of the Electrical Conductivity and Viscosity on the Motions inside Taylor Cone," *Journal of Electrostatics,* vol. 47, pp. 13-26, 1999.

[38] M. M. Hohman, M. Shin, G. Rutledge and M. P. Brenner, "Electrospinning and electrically forced jets. I. Stability theory," *Physics of Fluids,* vol. 13, no. 2201, 2001.

[39] R. Nayak, R. Padhye, I. L. Kyratzis, Y. B. Truong and L. Arnold, "Effect of viscosity and electrical conductivity on the morphology and fiber diameter in melt electrospinning of polypropylene," *Textile Research Journal,* vol. 83, no. 6, pp. 606-617, 2013.

[40] I. Roghair, M. Musterd, D. Ende, C. Kleijin, M. Kruetzer and F. Mugele, "A Numerical Technique to Simulate Display Pixels Based on Electrowetting," *Microfluidics and Nanofluidics,* vol. 19, pp. 465-482, 2015.

[41] H. Huh and R. E. Wirz, "Numerical Simulation of Electrospray Extraction for Highly Conductive Propellants," in *36th International Electric Propulsion Conference, IEPC-2019-565*, University of Vienna, Austria, 2019.

[42] M. Gamero-Castaño, "The Structure of Electrospray Beams in Vacuum," *Journal of Fluid Mechanics,* vol. 604, pp. 339-368, 2008.

[43] C.-H. Chen, "Electrohydrodynamic Stability," in *Electrokinetics and Electrohydrodynamics in Microsystems*, Springer, 2011, pp. 177-220.

[44] P. L. Wright, H. Huh, N. M. Uchizono, A. Thuppul and R. E. Wirz, "A Novel Variable Mode Emitter for Electrospray Thrusters," in *36th International Electric Propulsion Conference*, Vienna, Austria, 2019.

[45] R. E. Wirz, J. Polk, C. Marrese, J. Mueller, J. Escobendo and P. Sheehan, "Development and Testing of a 3 cm Electron Bombardment Micro-Ion Thruster," in *International Electric Propulsion Conference*, Pasadena, 2001.

[46] R. E. Wirz, J. Polk, C. Marrese and J. Mueller, "Experimental and Conputational Investigation of the Performance of Micro-Ion Thruster," in *AIAA Joint Propulsion Conference*, Indianapolis, 2002.

[47] R. E. Wirz, D. Goebel, C. Marrese and J. Mueller, "Development of Cathode Technologies for a Miniature Ion Thruster," in *39th AIAA Joint Propulsion Conference*, Huntsville, 2003.

[48] R. E. Wirz, M. Gamero and D. Goebel, "Pulsed Operation of an Ion Accelerator," NASA Tech Brief, Pasadena, 2009.

[49] R. Moore, "Magneto-electrostatically contained plasma ion thruster," in *7th Electric Propulsion Conference*, 1969.

[50] R. E. Wirz, "Miniature Ion Thrusters: A Review of Modern Technologies and Mission Capabilities," in *34th International Electric Propulsion Conference*, Kobe, Japan, 2015.

[51] S. Martin, D. P. Scharf, W. R. E., O. Lay, D. McKinstry, B. Mennesson, G. Purcell, J. Rodrugiez, L. Scherr, J. R. Smith and L. Wayne, "Design Study for a Planet-Finding Space Interferometer," in *IEEE Aerospace Conference*, 2008.

[52] M. J. Davis, A. L. Collins and R. E. Wirz, "Electrospray Plume Evolution Via Discrete Simulations," in *International Electric Propulsion Conference IEPC-2019-590*, Austria, 2019.